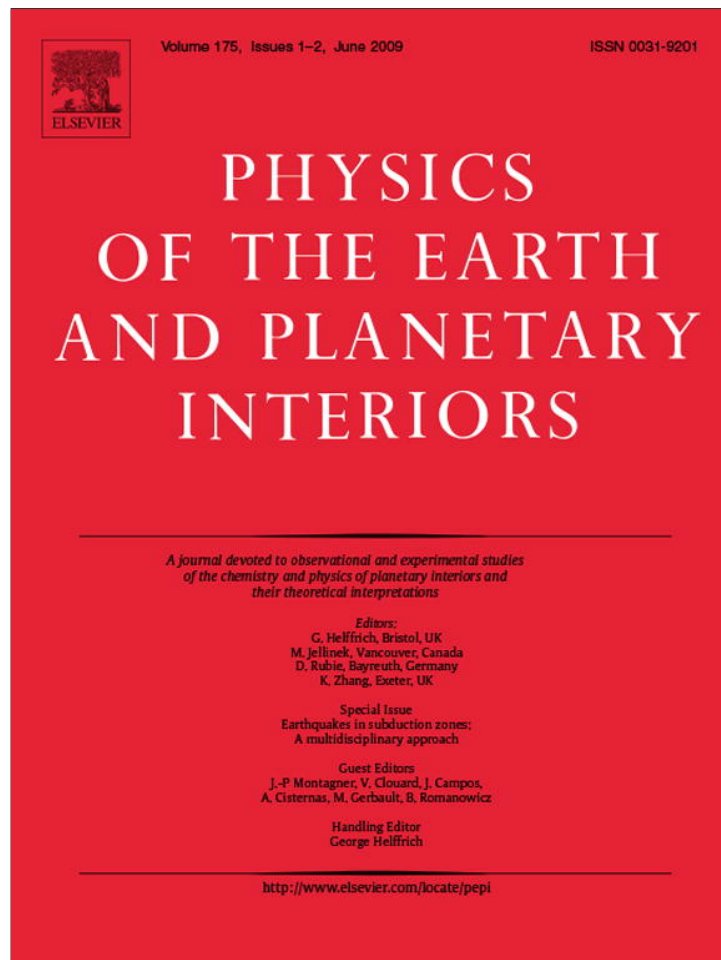


Provided for non-commercial research and education use.
Not for reproduction, distribution or commercial use.



This article appeared in a journal published by Elsevier. The attached copy is furnished to the author for internal non-commercial research and education use, including for instruction at the authors institution and sharing with colleagues.

Other uses, including reproduction and distribution, or selling or licensing copies, or posting to personal, institutional or third party websites are prohibited.

In most cases authors are permitted to post their version of the article (e.g. in Word or Tex form) to their personal website or institutional repository. Authors requiring further information regarding Elsevier's archiving and manuscript policies are encouraged to visit:

<http://www.elsevier.com/copyright>



Contents lists available at ScienceDirect

Physics of the Earth and Planetary Interiors

journal homepage: www.elsevier.com/locate/pepi

Interseismic strain accumulation measured by GPS in the seismic gap between Constitución and Concepción in Chile

J.C. Ruegg^{a,*}, A. Rudloff^b, C. Vigny^b, R. Madariaga^b, J.B. de Chabali^a, J. Campos^c, E. Kausel^c, S. Barrientos^c, D. Dimitrov^d

^a Institut de Physique du Globe (IPGP), Paris, France

^b Laboratoire de Géologie, Ecole Normale Supérieure (ENS), CNRS, Paris, France

^c Departamento de Geofísica (DGF), Universidad de Chile, Santiago, Chile

^d Bulgarian Academy of Sciences, Sofia, Bulgaria

ARTICLE INFO

Article history:

Received 30 March 2007

Accepted 10 February 2008

Keywords:

GPS

Tectonics

Seismic gap

Subduction

Coupling

ABSTRACT

The Concepción–Constitución area [35–37°S] in South Central Chile is very likely a mature seismic gap, since no large subduction earthquake has occurred there since 1835. Three campaigns of global positioning system (GPS) measurements were carried out in this area in 1996, 1999 and 2002. We observed a network of about 40 sites, including two east–west transects ranging from the coastal area to the Argentina border and one north–south profile along the coast. Our measurements are consistent with the Nazca/South America relative angular velocity (55.9°N, 95.2°W, 0.610°/Ma) discussed by Vigny et al. (2008, this issue) which predicts a convergence of 68 mm/year oriented 79°N at the Chilean trench near 36°S. With respect to stable South America, horizontal velocities decrease from 45 mm/year on the coast to 10 mm/year in the Cordillera. Vertical velocities exhibit a coherent pattern with negative values of about 10 mm/year on the coast and slightly positive or near zero in the Central Valley or the Cordillera. Horizontal velocities have formal uncertainties in the range of 1–3 mm/year and vertical velocities around 3–6 mm/year. Surface deformation in this area of South Central Chile is consistent with a fully coupled elastic loading on the subduction interface at depth. The best fit to our data is obtained with a dip of $16 \pm 3^\circ$, a locking depth of 55 ± 5 km and a dislocation corresponding to 67 mm/year oriented 78°N. However in the northern area of our network the fit is improved locally by using a lower dip around 13° . Finally a convergence motion of about 68 mm/year represents more than 10 m of displacement accumulated since the last big interplate subduction event in this area over 170 years ago (1835 earthquake described by Darwin). Therefore, in a worst case scenario, the area already has a potential for an earthquake of magnitude as large as 8–8.5, should it happen in the near future.

© 2009 Elsevier B.V. All rights reserved.

1. Introduction

The coastal ranges of Chile are among the most seismically active zones in the world. On average, one major earthquake of magnitude 8 has occurred every 10 years in historical times, and most of the individual segments of the coastal ranges have been the site of at least one magnitude 8 during the last 130 years (Lomnitz, 1971; Kelleher, 1972; Nishenko, 1985). One exception is the South Central Chile region, between 35°S and 37°S, which experienced its last large subduction earthquake on 20 February 1835 (Darwin, 1851) with an estimated magnitude close to 8.5 (Lomnitz, 1971; Beck et al., 1998) (Fig. 1). This area lies immediately to the north of the rupture zone associated with the great 1960 earthquake, of magnitude

9.5 (Plafker and Savage, 1970; Cifuentes, 1989) and south of the rupture zones corresponding to the 1928 Talca earthquake (Beck et al., 1998) and the 1906 and 1985 Valparaiso earthquakes (Barrientos, 1995). Part of the region was affected by the 1939 Chillán earthquake (magnitude 7.9). Recent studies have demonstrated that this event was not a typical subduction earthquake, but was a slab-pull event due to the release of tensional stresses within the downgoing slab (Campos and Kausel, 1990; Beck et al., 1998). Further north, the Talca earthquake of 1 December 1928, was interpreted as a shallow dipping thrust event (Lomnitz, 1971; Beck et al., 1998). Despite the uncertainties that remain on the importance of the 1928 and 1939 earthquakes and their impact on the seismic cycle, the region from 35°S to 37°S is a likely spot for a major subduction earthquake in the coming decades. In any case, it is the longest standing gap in Chile, the better known northern Chile gap was affected by large earthquakes in 1868 and 1877 (Lomnitz, 1971; Kelleher, 1972).

* Corresponding author.

E-mail address: ruegg@ipgp.jussieu.fr (J.C. Ruegg).

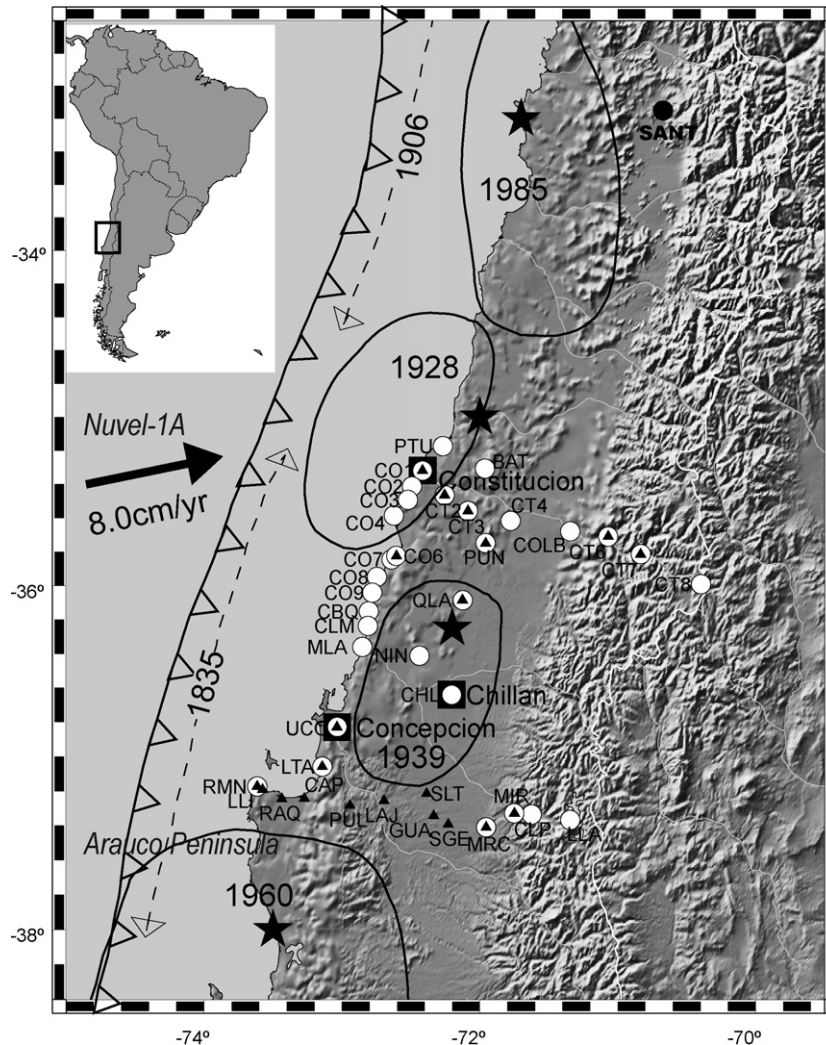


Fig. 1. Location of stations of the South Central Chile GPS experiment with respect to the seismotectonic context: open circles show location of GPS stations implanted in December 1996 and black triangles in March 1999. All stations were re-measured in April 2002. Black stars show the epicentres of the 1928, 1939, 1960 and 1985 earthquakes and large ellipses delimit the corresponding rupture zones. Dashed lines show the approximate extension of 1835 and 1906 earthquake ruptures. Plate convergence is from Nuvel-1A model (DeMets et al., 1994). Inset shows the location of the studied area in South America.

The area located immediately south of the city of Concepción between 37°S and 38°S is particularly interesting. The Arauco peninsula is an elevated terrace with respect to the mean coastal line. It shows evidences of both quaternary and contemporary uplift. Darwin (1851) reported 3 m of uplift at Santa Maria Island due to the 1835 earthquake. On the other hand, this area constitutes the limit between the rupture zones of the 1835 and 1960 earthquakes. As such, it might play an important role in the segmentation of the subducting slab. This tectonic situation is similar to that of the Mejillones Peninsula which seems to have acted as a limit to southward propagation for the 1877 large earthquake in Northern Chile, and to northward propagation during the 1995 Antofagasta earthquake (Armijo and Thiele, 1990; Ruegg et al., 1996).

The seismicity of the region remained largely unknown and imprecise because of the lack of a dense seismic network until a seismic field experiment that was carried out in 1996. The results of this experiment reveal the distribution of the current seismicity, focal mechanism solutions, and geometry of the subduction (Campos et al., 2002).

What is the potential for a future earthquake? How is the current plate motion accommodated by crustal strain in this area? In order to study the current deformation in this region, a GPS network was installed in 1996, densified in 1999 with nine new points

between the Andes mountains and the Arauco peninsula, and finally resurveyed entirely in 2002. A first estimation of the interseismic velocities in this area was done using the first two campaigns of 1996 and 1999 (Ruegg et al., 2002). We report here on the GPS measurements carried out in 1996, 1999 and 2002, and the interseismic velocities at 36 points sampling the upper plate deformation.

2. GPS measurements and data analysis

The GPS experiments began in 1996 with the installation of geodetic monuments at 33 sites distributed in three profiles and five other scattered points covering the so-called South Central Chile seismic gap between Concepción to the south and Constitución to the north. The northern transect, oriented 110°N, includes eight sites between the Pacific coast and the Chile–Argentina border (CO1, CT2, CT3, CT4, COLB, CT6, CT7, CT8) (Fig. 1). A coastal profile includes 11 sites between PTU north of the city of Constitución city and Concepción in the south. A southern profile, roughly oriented W–E was initiated between the Arauco peninsula, south of Concepción (two sites, RMN, LTA and four sites between the foothills of the Andes and the Chile–Argentina border MRC, MIR, CLP, LLA). Five additional points were located in the Central Valley area (BAT, PUN, QLA, NIN, CHL). During the first measurement campaign in Decem-

ber 1996 we used nine Ashtech Z12 with geodetic L1/L2 P antennas (ASHP12) and three Trimble SSE receivers with geodetic L1/L2 SSE antennas.

Eight new sites were installed during the March 1999 measurement campaign in the southern part of the 1996 network in order to complete the southern profile between the Arauco peninsula and the foothills of the Andes (LLI, RAQ, CAP, PUL, LAJ, SLT, SGE) (Fig. 1). We used seven Ashtech Z12 equipped with choke-ring antennas. At the same time, 13 points of the 1996 network were measured again, providing a first estimation of the interseismic velocity field (Ruegg et al., 2002). Most of the sites were equipped with brass benchmarks sealed in bedrock outcrops, but the measurements were done using tripods and optical tribrachs which enable centering with only sub-centimeter accuracy. However, most of the sites were equipped with three auxiliary points allowing a better permanency.

Finally almost the entire network was resurveyed in March 2002 using Ashtech Z12 equipped with choke-ring antennas. During all campaigns each site were measured for 12–24 h per day over 2–4 days, while three points (QLA, PUN, CO6) were measured continuously in 24-h sessions during 1 week.

Table 2
Site positions and velocities, in ITRF2000 and relative to South America plate. Latitude and longitude are in decimal degrees. All velocities and velocity uncertainties are in mm/year.

Site	Position		Velocity/ITRF2000		Velocity/SOAM		Uncertainties		
	Longitude	Latitude	Vlon	Vlat	Vlon	Vlat	s_lon	s_lat	Corr.
BAT	-71.962	-35.307	32.56	19.62	33.21	9.24	1.28	1.17	0.025
CAP	-73.272	-37.245	34.47	27.41	34.74	17.15	2.83	1.79	0.093
CHL	-72.205	-36.639	26.65	18.89	27.11	8.53	1.58	1.22	0.013
CLM	-72.812	-36.236	33.08	23.02	33.53	12.72	1.54	1.21	0.003
CLP	-71.625	-37.336	16.77	11.50	17.21	1.09	1.30	1.19	0.026
CO1	-72.415	-35.318	36.41	21.55	37.01	11.21	1.49	1.19	0.002
CO2	-72.491	-35.412	34.65	22.97	35.23	12.64	1.61	1.25	0.025
CO4	-72.626	-35.586	34.70	23.97	35.25	13.65	1.47	1.22	0.019
CO6	-72.606	-35.828	34.32	23.24	34.84	12.92	1.24	1.15	0.022
CO7	-72.639	-35.843	35.48	23.13	36.00	12.81	1.60	1.24	0.048
CO8	-72.744	-35.949	35.46	23.61	35.95	13.30	1.75	1.27	0.052
COLB	-71.347	-35.677	27.21	15.83	27.88	5.39	1.23	1.16	0.019
CT2	-72.255	-35.464	34.76	20.56	35.36	10.20	1.62	1.22	0.014
CT3	-72.086	-35.558	33.04	20.26	33.65	9.89	1.42	1.21	0.013
CT4	-71.777	-35.616	30.08	17.46	30.71	7.06	1.40	1.25	0.004
CT6	-71.069	-35.709	22.49	17.56	23.19	7.09	1.27	1.17	0.015
CT7	-70.834	-35.815	17.86	13.48	18.57	2.99	1.41	1.18	-0.002
CT8	-70.399	-35.991	9.84	11.34	10.58	0.81	1.23	1.10	0.033
GUA	-72.333	-37.346	22.92	16.56	23.28	6.21	2.60	1.97	0.232
LAJ	-72.697	-37.255	25.86	20.55	26.19	10.24	1.62	1.45	0.024
LLA	-71.344	-37.369	14.79	10.95	15.26	0.51	1.31	1.20	0.025
LLI	-73.569	-37.192	42.29	24.92	42.54	14.69	2.28	1.65	0.090
LTA	-73.142	-37.059	30.95	23.87	31.26	13.60	1.60	1.24	-0.003
MIR	-71.75	-37.330	16.54	12.60	16.97	2.20	1.41	1.22	0.033
MRC	-71.955	-37.411	18.62	14.02	19.01	3.64	1.30	1.19	0.026
NIN	-72.437	-36.410	34.76	15.56	35.23	5.22	1.28	1.17	0.020
PTU	-72.269	-35.172	32.02	22.88	32.66	12.53	1.37	1.18	0.032
PUL	-72.942	-37.285	30.16	21.03	30.46	10.74	1.62	1.45	0.027
PUN	-71.957	-35.750	31.30	19.90	31.90	9.52	1.24	1.16	0.021
QLA	-72.125	-36.085	29.87	18.28	30.41	7.91	1.23	1.15	0.021
RAQ	-73.436	-37.256	36.44	24.51	36.69	14.27	2.43	1.65	0.087
SGE	-72.231	-37.393	23.90	16.81	24.27	6.45	2.14	1.60	0.088
SLT	-72.384	-37.216	27.66	18.28	28.03	7.94	1.63	1.47	0.021
UCO	-73.035	-36.829	33.77	23.05	34.12	12.77	2.16	1.67	0.045
DGF	-70.664	-33.457	22.93	18.36	23.94	7.86	2.27	1.58	0.018
Permanent sites									
SANT	-70.669	-33.150	19.39	16.64	20.44	6.14	0.79	0.76	0.013
AREQ	-71.493	-16.466	14.20	14.89	17.12	4.46	4.50	2.80	0.075
BRAZ	-47.878	-15.947	-4.32	12.31	-0.08	0.64	1.00	1.00	0.000
EISL	-109.383	-27.148	66.00	-7.72	65.27	-12.70	0.92	0.89	-0.007
GALA	-90.304	-0.743	51.76	12.15	56.26	3.99	0.92	0.93	-0.012
KOUR	-52.806	5.252	-4.68	12.05	0.06	0.48	0.88	0.90	0.037
LPGS	-57.932	-34.907	-1.99	11.10	0.24	-0.28	0.83	0.81	-0.014
OHIG	-57.9	-63.321	14.58	9.71	14.24	-1.67	0.98	0.98	0.008
RIOG	-67.751	-53.785	3.27	11.59	2.28	0.84	0.88	0.90	-0.001

Table 1
Average short (<300 km) baseline repeatabilities (root mean square scatter about the mean) for each of the three campaigns. Values are in mm.

	December 1996	March 1999	April 2002
North rep.	3.8	2.4	2.5
East rep.	4.5	2.5	3.0
Vertical rep.	14.8	12.6	9.7

The current solution gives velocities at 36 sites determined over the 6 years period. We analyse the GPS data in 24-h sessions to give daily estimates of station position using the GAMIT software (King and Bock, 2000), choosing the ionosphere-free combination, and fixing the ambiguities to integer values. We use precise orbits from the International GPS Service for Geodynamics (IGS) (Beutler et al., 1993). We also use IGS Tables to describe the phase centers of the antennae. We estimate one tropospheric vertical delay parameter per station every 3 h. The horizontal components of the calculated relative position vectors (Table 1) are accurate to within a few millimetres for pairs of stations less than 300 km apart, as measured by the root mean square (RMS) scatter about the mean (the so-

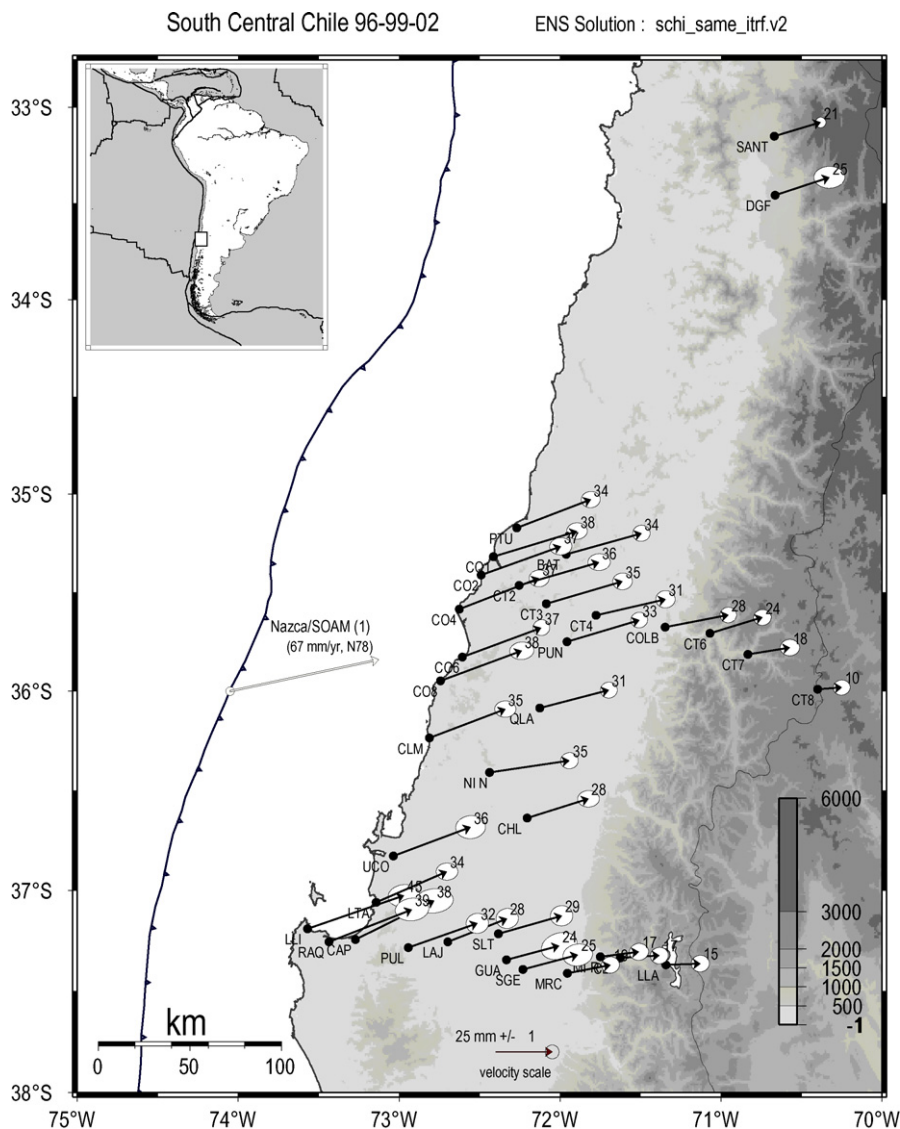


Fig. 2. South Central Chile experiment: GPS velocities relative to stable South America. Dots show locations of GPS stations. Arrows depict their horizontal velocities with respect to a reference frame fixed on the South America plate. Bold numbers beside the arrows indicate the velocity in mm/year. Ellipses depict the region of 99% confidence using the uncertainties in Table 2.

called baseline repeatability). Daily solutions were recalculated for the three epochs including tracking data from a selection of permanent stations (11 for the 2002 experiment) in South America, some of them belonging to the International GPS Service (IGS) (Neilan, 1995). Two stations are close to the deformation area, seven more span the South American craton in Brazil, Guyana and Argentina, and the remaining two samples the Nazca plate.

In the second step, we combine the daily solutions using the GLOBK Kalman filter software (Herring et al., 1990) in a “regional stabilization” approach. We combine daily solutions using Helmert-like transformations to estimate translation, rotation, scale and Earth orientation parameters (polar motion and UT1 rotation). This “stabilization” procedure defines a reference frame by minimizing, in the least-square sense, the departure from the prior values determined in the International Terrestrial Reference Frame (ITRF) 2000 (Altamimi et al., 2002). This procedure, described in more details in Vigny et al. (2008, this issue), estimates the positions and velocities for a set of 9 well-determined fiducial stations in and around our study area (AREQ, BRAZ, EISL, GALA, KOUR, LPGS, OHIG, RIOG, SANT). The misfit to these “stabilization” stations is 2.8 mm in position and 1.6 mm/year in velocity.

It is long recognized that without adding a proper noise model to GPS data processing we obtain unrealistic very low uncertainties on rates determined over long periods of time. This does not mean that the rate inferred from the time series is in error, but that its uncertainty is not correct. When using continuous measurements and daily time series, robust mathematical models of different kinds of noise (white noise, random-walk noise, flicker noise) can be tested and applied to the data (for a complete discussion see, e.g. Williams et al., 2004). Unfortunately, for survey mode measurements it is an impossible task to infer the noise model from the data themselves and we have to use *a priori* assumption on the noise nature. In our processing, this is done by adding a moderate random-walk type noise (2 mm/year^{1/2}) to the coordinates of stations when combining the daily solutions, following the procedures described in Herring et al. (1990) and Herring (1999). Applying this strategy leads to the estimation of more realistic velocity uncertainties (1–2 mm/year instead of the formal *a priori* value of 0.1–0.2 mm/year). However, although velocities do not change by more than ±1 mm/year at all sites, this procedure degrades the realization of the reference frame and the combination with subsets of stations measured at different epochs: It

simply also adds noise to the velocity field. Therefore we choose to estimate the velocity uncertainties with added random-walk noise, but to keep the velocities estimated without adding this noise model.

3. Velocity field

This procedure leads to horizontal velocities with respect to the ITRF2000 (Table 2). Here we present our results both in the ITRF2000, and relative to the South American plate by using the angular velocity of this plate (21.5°S , 134.6°W , $0.113^\circ/\text{Myr}$) in the ITRF2000. The results relative to the South American plate using this pole differ slightly from those of Vigny et al. (2009, this issue) who use the angular velocity (25.4°S , 124.6°W , $0.11^\circ/\text{Myr}$) given by the NNR-Nuvel-1A model (DeMets et al., 1994). First of all, far field stations spanning the South American craton show that the latter is not affected by any significant internal deformation. Second, stations on the Nazca plate (EISL and GALA) are also consistent with their reduced Nazca/South America angular velocity, which predicts 68 mm/yr of convergence oriented 78°N on the trench at the latitude of our network.

3.1. South Central Chile velocities

Fig. 2 depicts the velocity field with respect to the stable South America reference frame. Observed velocities decrease rapidly from the Pacific coast to the Chile–Argentina border, 200 km inland. Coastal stations move inland with velocities close to 35–40 mm/year while Andean stations move with a velocity closer to 10–20 mm/year. Accordingly, velocity directions rotate from their initial strike of $70 \pm 1^\circ\text{N}$ along the coast (LLI, UCO, CO6, PTU), to $75 \pm 2^\circ\text{N}$ in the central valley (SLT, CHL, QLA, CT4), and almost purely east trending in the Andes (LLA and CT8).

Because it is the longest profile and because it starts closer to the trench, the southern profile between the Arauco peninsula and the Andes is particularly interesting. The nearest point to the trench (LLI) show a velocity of 46 ± 2.3 mm/year, while the last point in the Andes (LLA), presents a velocity of 15 ± 1.3 mm/year (Fig. 3). This implies an accumulation of 30 mm/year over this 200 km long distance, or an integrated strain rate of 1.5×10^{-6} per year.

The northern profile between Constitución and the Andes shows slightly less compression: 37 ± 1.6 mm/year at CO2 or CO4 and 10 ± 1.2 mm/year at Laguna Maule (CT8) on the top of Andes near the Chile–Argentina border (Fig. 3). Along this northern profile, stations lying at the same distance from the trench have a velocity 10–25% larger than along the southern profile (Fig. 3). Accordingly, northern transect stations show a different crustal strain than southern stations: weaker in the first half (100–200 km from the trench) and stronger in the second half in the foothills of the Andes (200–300 km from trench) (Fig. 3). These patterns are consistent with the accumulation of elastic strain in the upper plate due to locking on the subduction interface with latitude-dependent dip angle (see Section 4).

Although less precisely determined, the vertical velocities exhibit a coherent pattern which, like the horizontal ones, is consistent with what is expected from standard elastic modelling. Vertical velocities of the coastal stations are negative (indicating subsidence) when those of the Central Valley are positive (indicating uplift) and those of the Andean range are essentially near zero (Fig. 4a). This is particularly true around the Arauco peninsula where distance to the trench is lower than 100 km, and where vertical velocities are negative and less than -10 mm/year, accordingly with the modelled curve (Fig. 4b).

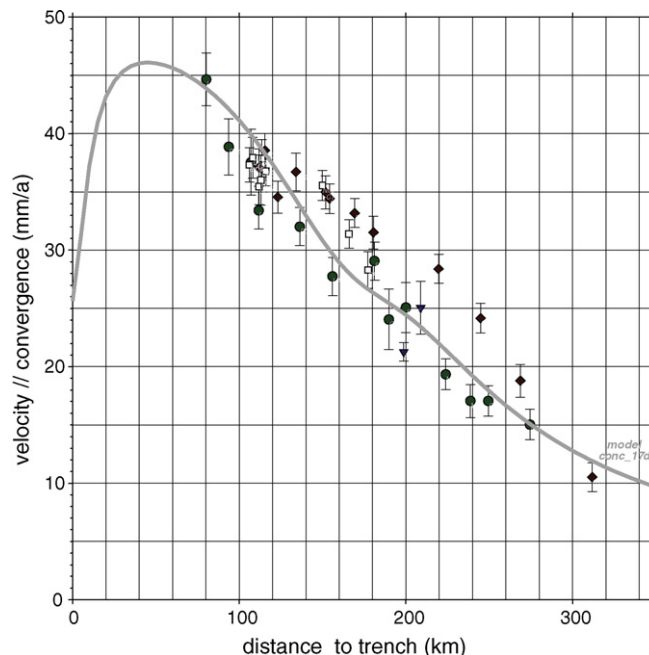


Fig. 3. Parallel velocity: cross section of the velocity parallel to the convergence direction versus the distance to the trench. Black diamonds are for northern area points. Black dots are for southern transect and open square for other distributed points between the two transects. The grey line shows the horizontal parallel velocity predict by our best model described in Fig. 5.

4. Elastic modelling

To model the upper plate deformation during the interseismic stage, we make the usual assumption that the interface between the Nazca and South American plates is locked down to a certain depth (the locking depth or coupling depth), while the deeper part is slipping continuously at the relative plate velocities. This corresponds to the “seismically coupled zone”, portion of the upper plate interface which might be the site of a future major thrust earthquake in the BioBío and Maule regions of Chile. We model this deformation using a simple back-slip assumption (Savage, 1983) for which the interseismic accumulation correspond exactly to the released co-seismic deformation (with reversed sign), and we use Okada’s elastic model to relate the surface deformation to the dislocation buried at depth (Okada, 1985). We define the geometry of the fault plane model by considering the distribution of earthquakes (Campos et al., 2002) and the slab geometry as given by Cahill and Isacks (1992). The fault plane model is simply defined by nine parameters: three for the location of the fault’s center, azimuth (strike), dip, width along the dip and length of the fault plane, and finally the slip dislocation vector (slip modulus and rake angle). A strike angle of about $\text{N}19^\circ\text{E}$ is chosen in agreement with the average direction of both the trench axis and the coast line between 33°S and 38°S . A dip angle of 20° is taken for our first trial model but our final model uses a dip of 17° . The up-dip limit of our fault plane is taken to be at the trench, at a depth of 6 km. The center of the fault model is taken at the average latitude of the observed sites (37°S) and the length of the model extends for a distance of 1000 km along the coast to avoid edge effects. We used the parameters defining the convergence at the trench, 68 mm/year in the direction 78°N , to define the slip vector of the model and the corresponding rake (here -59° for a back slip model).

In our trial models, we fixed six parameters of the well known geometry of the subduction and left only free the dip, the width along the dip, and the slip modulus. The goodness of fit of the model is estimated by calculation of the mean residual (mean absolute

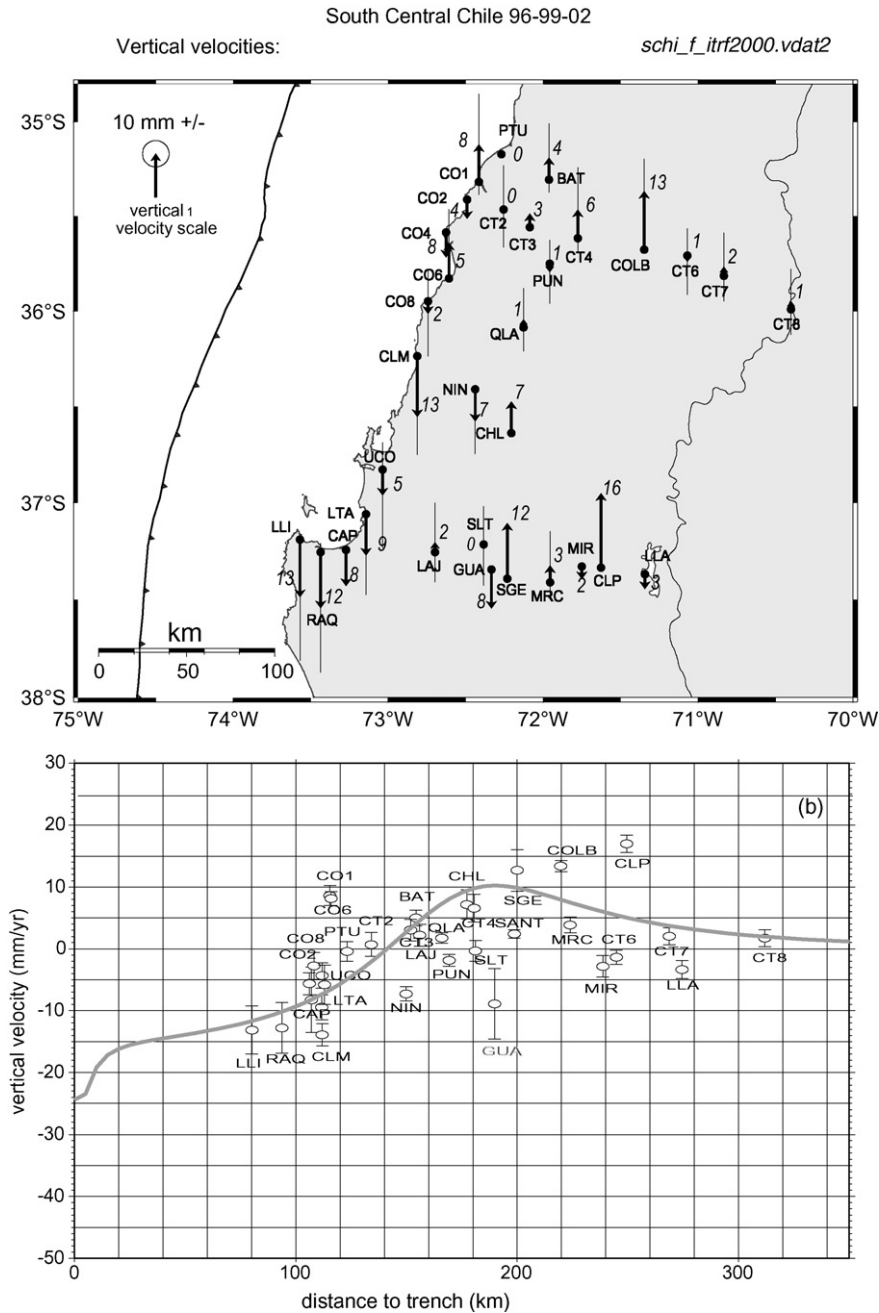


Fig. 4. Vertical component of the displacement. (a) Map of vertical velocities; (b) vertical velocities in mm/year versus the distance to the trench of each station. The grey line shows the vertical component of the model described in Fig. 5.

error) between observed and modeled vectors. We explored the dip angle between 12° and 22° , the width (W) between 150 and 250 km, and the slip between 35 and 67 mm/year, i.e. the range of 50–100% coupling.

Considering the whole set of observed points, the best fit is obtained with a fault plane of $17 \pm 2^\circ$ dip, and a locking depth of 58 ± 6 km located at a distance of 180 km eastwards from the trench and a slip of 67 mm/year. In this case the mean residual is 3.4 ± 0.2 mm/a.

One point NIN0 shows an anomalous residual vector of about 10 mm/year, because a shift on the direction of the observed vector probably due to a movement of the monument.

If we consider separately the southern area, south of the city of Chillan (36.5° S) and the northern one ($35\text{--}36^\circ$ S), we obtain the following results:

- Southern area: dip $18 \pm 2^\circ$, a width of 180 km, a locking depth: 61 ± 3 km, a mean residual: 2.1 ± 0.4 mm/a, and a 100% coupling, i.e. values very near from those of the whole set of points.
- For the northern area we found two minimum: one with values very near from those of the whole set of points: dip $17 \pm 2^\circ$, width 180 km, locking depth: 61 ± 9 km, mean residual: 4.0 ± 0.4 mm/a, and a 100% coupling; but a second solution and slightly better solution is obtained with a slip of about 54 mm/year (78% coupling); dip $13 \pm 1^\circ$, width 250 km, locking depth: 62 ± 1 km, which fits with a mean residual of 2.8 ± 0.1 mm/a.

These results mean that at the first order the interface is fully locked, or in other words that the coupling between the two plates is 100%. This result is in agreement with those of Khazaradze and Klotz (2003) who find a similar locking depth and full coupling (100%).

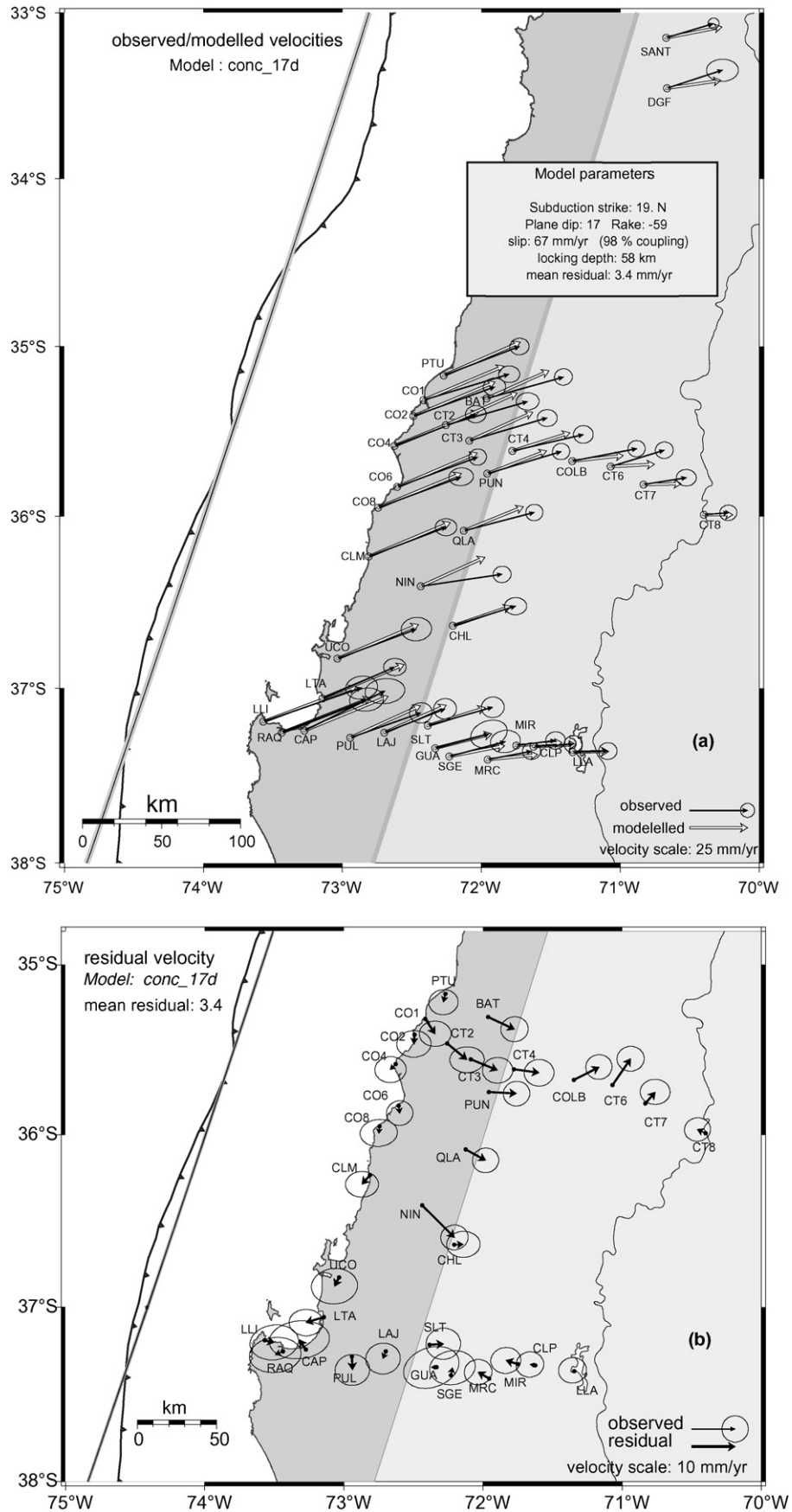


Fig. 5. Elastic modelling of the upper plate deformation in the South Central Chile gap. (a) GPS observations (brown arrows) and model predictions (white arrows) are shown. Inset describes the characteristics of the model. (b) Residual (i.e. observations-model) velocities are shown (black arrow). In both boxes, the grey contour line and shaded pattern draw the subduction plane buried at depth and the white arrows depict the dislocation applied on this plane.

The worse fit observed in the northern area of our study could be due to either a different dip angle of the subduction interface, a variation in the dip with distance from the trench, or a change in the locking depth. Indeed, the fit can be improved locally by using a slightly reduced dip angle of 13° , which generates a longer slab before it reaches the depths at which it starts to slip freely. The usage of a shallower and longer slab generates an eastward shift of the deformation gradient, such as the one observed in our data (Fig. 3).

5. Conclusion

In this paper we extend the finding of preliminary results obtained with only two GPS campaigns and a lower number of observed sites (Ruegg et al., 2002). Interseismic velocities (horizontal and vertical components) have been determined at 36 sites (against 13 in Ruegg et al., 2002), with better uncertainties (formal uncertainties in the range of 1–3 mm/year and vertical velocities around 3–5 mm/year). The velocities on the northern transect vary from 36 mm/year at the coast and 10 mm/year at the Chile–Argentina border, with a particularly high gradient of velocity from the foothills of the Andes to their top (0.5×10^{-6} linear strain per year at 220–320 km from trench). The southern transect exhibits very high geodetic speed in the coastal region of Arauco (45 mm/year) which decrease to 15 mm/year at the top of the Andes which implies a strong strain accumulation of 1.5×10^{-6} per year over this 200 km long distance between the coast and the top of the Andes. Vertical velocities are negative at the coast, while those measured in the Central Valley have positive values and those on the Andean range are close to zero.

This deformation pattern is very well explained by the elastic loading of the seismogenic zone of the plate interface by continuous slip at depth, using as slip vector the convergence rate between the two plates (68 mm/year at 78°N). Thus, it appears that at first order the plates are fully coupled with a locking depth situated at 60 ± 5 km depth at a distance of 180 km from trench. We do not know whether the plate interface has slipped episodically in the past, or whether it has remained fully locked since the last big earthquake 1835. In the worst case scenario, that strains have not been relieved at all since 1835, at a convergence rate of 68 mm/year more than 10 m of slip deficit will have accumulated since 1835. It is possible that the northern part of the plate interface between Constitución and Concepción was affected by the earthquakes of 1851, 1928 and 1939, but it is unlikely that this was the case near the city of Concepción. We would then conclude that the southern part of the Concepción–Constitución gap has accumulated a slip deficit that is large enough to produce a very large earthquake of about $M_w = 8.0$ – 8.5 . This is of course a worst case scenario that needs to be refined by additional work.

Acknowledgments

This work is part of a cooperative project between Universidad de Chile, Santiago, Institut de Physique du Globe de Paris and Ecole Normale Supérieure, Paris. It was initiated by a European Community contract C11-CT94-0109 and supported by the French Ministère

des Affaires Etrangères (comité ECOS), by CNRS/INSU programs (ACI CatNat) and by “Nucleo Milenio en Sismotectónica y Peligro Sísmico”. We are grateful to many people who participated in measurement campaigns, and particularly our colleagues H. Lyon-Caen, E. Clevede and T. Montfret, as well as students from DGF and ENS.

References

- Altamimi, Z., Sillard, P., Boucher, C., 2002. ITRF2000: a new release of the International Terrestrial Reference frame for earth science applications. *J. Geophys. Res.* SA107 (B10) (Art. no. 2214).
- Armijo, R., Thiele, R., 1990. Active faulting in northern Chile: ramp stacking and lateral decoupling along a subduction plate boundary? *Earth Planet. Sci. Lett.* 98, 40–61.
- Barrientos, S.E., 1995. Dual seismogenic behavior: the 1985 Central Chile earthquake. *Geophys. Res. Lett.* 22, 3541–3544.
- Beck, S., Barrientos, S., Kausel, E., Reyes, M., 1998. Source characteristics of historic earthquakes along the central Chile subduction zone. *J. S. Am. Earth Sci.* 11, 115–129.
- Beutler, G., Kouba, J., Springer, T., 1993. Combining the orbits of the IGS processing centers. In: Kouba, J. (Ed.), *Proceedings of the IGS Analysis Center Workshop*, pp. 20–56.
- Cahill, T., Isacks, B., 1992. Seismicity and shape of the subducted Nazca plate. *J. Geophys. Res.* 97, 17503–17529.
- Campos, J., Kausel, E., 1990. The large 1939 intraplate earthquake of Southern Chile. *Seis. Res. Lett.*, 61.
- Campos, J., Hatzfeld, D., Madariaga, R., López, G., Kausel, E., Zollo, A., Iannaccone, G., Fromm, R., Barrientos, S., Lyon-Caen, H., 2002. A seismological study of the 1835 seismic gap in South Central Chile. *Phys. Earth Planet. Int.* 132, 177–195.
- Cifuentes, I.L., 1989. The 1960 Chilean earthquake. *J. Geophys. Res.* 94, 665–680.
- Darwin, C., 1851. *Geological Observations on Coral Reefs, Volcanic Islands and on South America*. Londres, Smith, Elder and Co, p. 768.
- DeMets, C., et al., 1994. Effect of the recent revisions to the geomagnetic reversal time scale on estimates of current plate motions. *Geophys. Res. Lett.* 21, 2191–2194.
- Herring, T.A., Davis, Shapiro, 1990. *Geodesy by radio interferometry: the application of Kalman filtering to the analysis of very long baseline interferometry data*. *J. Geophys. Res.* 95, 12561–12581.
- Herring, T.A., 1999. *Documentation for the GLOBK Software Version 5.01*. Mass. Inst. of Technol., Cambridge.
- Kelleher, J., 1972. Rupture zones of large South American earthquakes and some predictions. *J. Geophys. Res.* 77, 2087–2103.
- Khazaradze, G., Klotz, J., 2003. Short and long-term effects of GPS measured crustal deformation rates along the South-Central Andes. *J. Geophys. Res.* 108 (B4), 1–13.
- King, R.W., Bock, Y., 2000. *Documentation for the GAMIT GPS Software Analysis Version 9.9*. Mass. Inst. of Technol., Cambridge.
- Lomnitz, C., 1971. Grandes terremotos y tsunamis en Chile durante el periodo 1535–1955. *Geofis. Panamericana* 1, 151–178.
- Neilan, R., 1995. The evolution of the IGS global network, current status and future aspects. In: Zumberge, J.F., et al. (Eds.), *IGS Annual Report*. JPL Publ. 95-18, pp. 25–34.
- Nishenko, R., 1985. Seismic potential for large and great intraplate earthquakes along the Chilean and Southern Peruvian margins of South America: a quantitative reappraisal. *J. Geophys. Res.* 90, 3589–3615.
- Okada, Y., 1985. Surface deformation due to shear and tensile faults in a half-space. *Bull. Seism. Soc. Am.* 75, 1135–1154.
- Plafker, G., Savage, J.C., 1970. Mechanism of the Chilean earthquake of May 21 and 22 1960. *Geol. Soc. Am. Bull.* 81, 1001–1030.
- Ruegg, J.C., Campos, J., Armijo, R., Barrientos, S., Briole, P., Thiele, R., Arancibia, M., Canuta, J., Duquesnoy, T., Chang, M., Lazo, D., Lyon-Caen, H., Ortlieb, L., Rossignol, J.C., Serrurier, L., 1996. The $M_w = 8.1$ Antofagasta earthquake of July 30 1995: first results from teleseismic and geodetic data. *Geophys. Res. Lett.* 23 (9), 917–920.
- Ruegg, J.C., Campos, J., Madariaga, R., Kausel, E., DeChabaliere, J.B., Armijo, R., Dimitrov, D., Georgiev, I., Barrientos, S., 2002. Interseismic strain accumulation in south central Chile from GPS measurements, 1996–1999. *Geophys. Res. Lett.* 29 (11), doi:10.1029/2001GL013438.
- Savage, J.C., 1983. A dislocation model of strain accumulation and release at a subduction zone. *J. Geophys. Res.* 88, 4948–4996.
- Vigny, C., Rudloff, A., Ruegg, J.-C., Madariaga, R., Campos, J., Alvarez, M., 2009. Upper plate deformation measured by GPS in the Coquimbo Gap, Chile. *PEPI* 175, 86–95.
- Williams, S.D.P., Bock, Y., Fang, P., Jamason, P., Nikolaidis, R.M., Prawirodirdjo, L., Miller, M., Johnson, D.J., 2004. Error analysis of continuous GPS position time series. *J. Geophys. Res.* 109, B03412, doi:10.1029/2003JB0022741.